Published in final edited form as:
Biochemistry. 2008 February 19; 47(7): 2143–2152. doi:10.1021/bi701879g.

Synaptotagmin Perturbs the Structure of Phospholipid Bilayers†

Victor Shahin[‡,§], **Debajyoti Datta**[‡], **Enfu Hui**[‖], **Robert M. Henderson**[‡], **Edwin R. Chapman**[‖], and **J. Michael Edwardson**[*,‡]

[‡]Department of Pharmacology, University of Cambridge, Tennis Court Road, Cambridge CB2 1PD, United Kingdom

[‖]Howard Hughes Medical Institute and Department of Physiology, University of Wisconsin School of Medicine, Madison, Wisconsin 53706

Abstract

Synaptotagmin I (syt), an integral protein of the synaptic vesicle membrane, is believed to act as a Ca^{2+} sensor for neuronal exocytosis. Syt's cytoplasmic domain consists largely of two C2 domains, C2A and C2B. In response to Ca^{2+} binding, the C2 domains interact with membranes, becoming partially embedded in the lipid bilayer. We have imaged syt C2AB in association with lipid bilayers under fluid, using AFM. As expected, binding of C2AB to bilayers required both an anionic phospholipid [phosphatidylserine (PS)] and Ca^{2+}. C2AB associated with bilayers in the form of aggregates of varying stoichiometries, and aggregate size increased with an increase in PS content. Repeated scanning of bilayers revealed that as C2AB dissociated it left behind residual indentations in the bilayer. The mean depth of these identations was 1.81 nm, indicating that they did not span the bilayer. Individual C2 domains (C2A and C2B) also formed aggregates and produced bilayer indentations. Binding of C2AB to bilayers and the formation of indentations were significantly compromised by mutations that interfere with binding of Ca^{2+} to syt or reduce the positive charge on the surface of C2B. We propose that bilayer perturbation by syt might be significant with respect to its ability to promote membrane fusion.

Neurotransmitter release occurs in response to Ca^{2+} influx across the presynaptic plasma membrane (1). There is persuasive evidence that a major Ca^{2+} sensor at most nerve terminals is synaptotagmin I (syt),[1] an integral protein of the synaptic vesicle membrane (reviewed in refs 2 and 3). The cytoplasmic region of syt consists predominantly of two C2 domains, known as C2A and C2B, which bind three and two Ca^{2+} ions, respectively (4, 5). In response to Ca^{2+} binding, syt interacts both with negatively charged phospholipids, such as phosphatidylserine (PS) (5–11) and phosphatidylinositol 4,5-bisphosphate (PIP_2) (12–14), and with soluble *N*-ethylmaleimide-sensitive fusion protein attachment protein receptors (SNAREs), proteins known to be key players in the process of membrane fusion (15–18). It is likely that the Ca^{2+}-triggered binding of syt to both phospholipids and SNAREs is essential for its function as a Ca^{2+} sensor for neurotransmitter release (19–24).

†This work was supported by Grant B19797 from the Biotechnology and Biological Sciences Research Council (to J.M.E. and R.M.H.) and grants from the NIH (NIGMS Grant GM 56827 and NIMH Grant MH61876) and the AHA (0440168N) to E.R.C. E.R.C. is an Investigator of the Howard Hughes Medical Institute. V.S. was supported by Grant SH 520404 from the Innovative Medical Research (Innovative Medizinische Forschung) of the medical faculty of Münster University (Münster, Germany). D.D. was supported by the Gates Cambridge Trust.

[*]To whom correspondence should be addressed. Phone: 44-1223-334014. Fax: 44-1223-334100. jme1000@cam.ac.uk.
[§]Current address: Institute of Physiology II, University of Münster, Robert-Koch-Str. 27b, D-48149 Münster, Germany.

[1]Abbreviations: AFM, atomic force microscopy; DOPC, dioleoylphosphatidylcholine; PE, phosphatidylethanolamine; PIP_2, phosphatidylinositol 4,5-bisphosphate; PS, phosphatidylserine; syt, synaptotagmin.

The interaction of syt with phospholipids has been the subject of numerous studies. It is now accepted that both C2A and C2B domains undergo Ca^{2+}-triggered association with negatively charged phospholipids (5–14). Furthermore, C2AB can cause Ca^{2+}-dependent clustering of liposomes (24–26). The association of syt with phospholipids is intimate, involving the penetration of the Ca^{2+} binding regions of the C2 domains into the lipid bilayer (9–11, 13, 18, 27–30) and also the induction of positive curvature in the bilayer (26, 31). Since membrane fusion requires a significant perturbation of the bilayers of the two interacting membranes, it seems likely that these effects of the C2 domains on the bilayer are physiologically significant.

Studies of the interaction of syt with lipid bilayers (e.g., binding to liposomes in suspension) have generated much information (5–14, 18, 26, 27); however, such studies are unable to provide much insight into either the form in which syt binds to the bilayer or the effect of this binding on the bilayer structure. Imaging experiments that have yielded structural information about the association of syt with phospholipids have so far been carried out under nonphysiological conditions, for example, electron microscopic analysis of the binding of syt to lipid monolayers in vacuo (32). Consequently, we are still some way from understanding how syt interacts with membranes in vivo.

In this study, we imaged the binding of syt to supported lipid bilayers under fluid using atomic force microscopy (AFM). This technique provides the opportunity to study the behavior of syt at the single-molecule level. We show that C2AB binds to lipid bilayers containing negatively charged phospholipid (PS) in a Ca^{2+}-dependent manner. Bound syt forms aggregates but does not seem to adopt a single stoichiometry. Intriguingly, the binding of C2AB induces the formation of stable indentations in the bilayer, suggesting that it is able to significantly perturb the bilayer structure. The possible significance of this perturbation with respect to Ca^{2+}-triggered membrane fusion is discussed.

EXPERIMENTAL PROCEDURES

DNA Constructs

cDNAs encoding the syt cytoplasmic domain (C2AB, residues 96–421), the C2A domain (residues 96–265), and the C2B domain (residues 248–421) were expressed as GST-tagged proteins and cleaved with thrombin, as described previously (32). A C2AB mutant in which aspartate residues crucial to binding of Ca^{2+} to both C2A and C2B (D230, -232, -363, and -365) had been neutralized by conversion to asparagines, designated $C2A_M$–$C2B_M$ (11, 13, 22, 23, 32), and C2AB harboring a mutation in C2B in which two lysine residues in a normally positively charged region (K326–K327) had been replaced with alanines, designated C2AB(KK) (11, 13, 22, 32), were also used. For all experiments, bacterial contaminants were removed from recombinant proteins by treatment with 1 M NaCl and RNase/DNase, as described previously (32).

Formation of Supported Lipid Bilayers

1,2-Dioleoyl-*sn*-glycero-3-phosphatidylcholine (DOPC) and brain L-α-PS, obtained from Avanti Polar Lipids (Birmingham, AL) as chloroform stocks, were mixed as appropriate. The chloroform was evaporated under a stream of nitrogen gas, and the lipids were rehydrated overnight in water (from a Millipore water purification system) to give a total lipid concentration of 2 mg/mL. The lipid mixture was vortexed to produce large multilamellar vesicles, from which small unilamellar vesicles were prepared by sonication in a heated (50 °C) bath sonicator (Decon Laboratories, Hove, U.K.) for 30 min. For the imaging of supported lipid bilayers, 10 μL of the vesicle suspension was added to 50 μL of HEPES-buffered saline (HBS) [100 mM NaCl and 20 mM HEPES (pH 7.6)], containing

either 500 μM $CaCl_2$ or 2 mM EGTA. The resulting suspension was deposited onto freshly cleaved mica (12.7 mm diameter disks; Agar Scientific) fixed by epoxy (Aron Alpha type 102, Agar Scientific) to 15-mm steel SPM specimen discs (Agar Scientific). After a 30-min adsorption on mica, the sample was rinsed with HBS to remove unadsorbed liposomes and then transferred to the atomic force microscope.

AFM Imaging

AFM imaging was carried out at room temperature (20 °C) using a Digital Instruments Multimode atomic force microscope equipped with a J-scanner and a Nanoscope IIIa controller with an in-line electronics extender module (Veeco/Digital Instruments, Santa Barbara, CA). All images were collected using tapping mode in fluid and using oxide-sharpened silicon nitride probes (DNP-S; Veeco/Digital Instruments). The V-shaped cantilevers (typically exhibiting a spring constant of 0.58 N/m and an estimated curvature radius of 10 nm) were tuned to 10–20% below the peak of the resonance frequency, generally found between 7.5 and 9 kHz. The drive amplitude was set to generate a root-mean-square amplitude of 0.3–0.6 V. The microscope was engaged with a 0-nm scan area to allow for tuning and a setpoint adjustment of 100–200 nm above the surface before scanning of the sample was performed. The setpoint was adjusted to the highest setting that allowed imaging with little noise, to minimize the force applied to the sample. Images were captured at a scan rate of 1 Hz (unless otherwise noted), and with 512 scan lines per area. Data analysis was performed using commercially available software (Nano-Scope III software, Digital Instruments; Scanning Probe Image Processor, Image Metrology, Lyngby, Denmark).

Determination of Molecular Volumes

The molecular volumes of the protein particles were determined from particle dimensions based on AFM images. The particles tend to adopt the shape of a spherical cap. The heights and half-height radii were measured from multiple cross sections of the same particle, and the molecular volume was calculated using the following equation

$$V_m=(\pi h/6)(3r^2+h^2) \quad (1)$$

where h is the particle height and r is the radius.

Molecular volume based on molecular mass was calculated using the equation

$$V_c=(M_0/N_0)(V_1+dV_2) \quad (2)$$

where M_0 is the molecular mass, N_0 is Avogadro's number, V_1 (0.74 cm^3/g) and V_2 (1 cm^3/g) are the partial specific volumes of the particle and water, respectively, and d (0.4 g of water/g of protein) is the extent of protein hydration (33).

Stopped-Flow Rapid Mixing Experiments

DOPC, synthetic 1,2-dioleoyl-*sn*-glycero-3-PS, and 1,2-dioleoyl-*sn*-glycero-3-phosphoethanolamine-*N*-(5-dimethylamino-1-naphthalenesulfonyl; dansyl-PE) were obtained from Avanti Polar Lipids. A phospholipid mixture, composed of 5% dansyl-PE, 25% PS, and 70% DOPC was dried and resuspended in HBS. Large (~100 nm) unilamellar liposomes were prepared by extrusion, as described previously (18).

Rapid mixing experiments were carried out using an Applied Photophysics (Leatherhead, U.K.) SX.18MV stopped-flow spectrometer. Ca^{2+}-dependent interactions between wild-type [C2AB(WT)] or mutant C2AB [C2AB(KK)] and PS-containing liposomes were monitored by fluorescence resonance energy transfer. Native tryptophan and tyrosine residues in C2AB (donors) were excited at 285 nm, and the fluorescence intensity of the dansyl-PE (acceptors) in liposome membranes was collected using a 470 nm band-pass filter. The dead time of the instrument was ~1.2 ms.

For the assembly experiments, increasing concentrations of liposomes were premixed with 0.2 mM Ca^{2+} and then rapidly mixed (1:1) with 4 μM C2AB. Single-exponential functions were used to determine the observed rate constants (k_{obs}) of Ca^{2+}-dependent C2AB-liposome interactions. The on- and off-rate constants (k_{on} and k_{off}, respectively) for the interaction of Ca^{2+}-C2AB with liposomes were calculated, assuming pseudo-first-order kinetics (18, 34): $k_{obs} = [\text{liposome}]k_{on} + k_{off}$. The dissociation constants (K_d) for C2AB–liposome interactions in the presence of Ca^{2+} were calculated as k_{off}/k_{on}. All experiments were carried out at 25.3 °C.

For the disassembly experiments, 44 nM liposomes (5% dansyl-PE/25% PS/70% PC) were premixed with 4 μM C2AB in the presence of 0.2 mM Ca^{2+} and then rapidly mixed with an equal volume of HBS buffer containing excess EGTA (2 mM). The chelation of Ca^{2+} by EGTA resulted in a rapid loss of the fluorescence signal. The rate constants for disassembly (k_{diss}) were estimated by fitting the kinetic traces using a single-exponential function. All experiments were carried out at 14.5 °C. (The disassembly of C2AB–liposome complexes was too fast to monitor when the temperature was ~25 °C.)

Statistical Analysis

All errors are reported as standard deviations (SD). The statistical significance of differences between groups was calculated using a Student's *t*-test for unpaired data.

RESULTS

We first imaged C2AB(WT) (2.5 nM) in association with mica, which presents a negatively charged surface at pH 7.6. As shown in Figure 1A, in the absence of Ca^{2+} (i.e., with 2 mM EGTA), C2AB appeared as a fairly homogeneous population of particles. The molecular volumes of a representative sample of particles were determined from the particle dimensions using eq 1, and a frequency distribution of volumes was produced (Figure 1B). The distribution was fitted well by a Gaussian curve, which had a peak at 103 nm^3. The size of a single C2AB molecule, predicted on the basis of a molecular mass of 42 kDa, is 80 nm^3 (eq 2). Hence, in the absence of Ca^{2+}, C2AB binds to mica predominantly as a monomer. When the experiment was repeated in the presence of Ca^{2+} (500 μM), the particles bound to mica appeared to be larger (Figure 1C). The frequency distribution of molecular volumes (Figure 1D) was now broader but was still fitted well by a Gaussian curve. The peak of the curve was now at 205 nm^3, double the molecular volume seen in the absence of Ca^{2+}. The simplest interpretation of this result is that, in the presence of Ca^{2+}, C2AB binds to mica predominantly as a dimer. Alternatively, Ca^{2+} could have caused a substantial conformational change in the protein, resulting in the presence of intramolecular cavities and a consequent overestimation of its volume. There is some evidence for a Ca^{2+}-induced conformational change in C2AB (35), but this does not seem to be large enough to account for the apparent change in molecular volume. We also tested the behavior of a C2AB mutant in which aspartate residues crucial to binding of Ca^{2+} to both C2A and C2B (D230, -232, -363, and -365) were neutralized by conversion to asparagines, designated $C2A_M$–$C2B_M$ (11, 13, 22, 23, 32). We found that this mutant was unable to dimerize in response to Ca^{2+}. The peaks of the molecular volume distributions for $C2A_M$–$C2B_M$ were at 107 nm^3 both in

the absence and in the presence of Ca^{2+}. Hence, Ca^{2+} needs to be able to bind to the C2 domains to trigger dimerization of C2AB on mica.

Clearly, the interaction of C2AB with mica has minimal physiological relevance. We therefore turned our attention to the interaction of C2AB with supported lipid bilayers under fluid, conditions that closely mimic those prevailing in vivo. Liposomes were produced and deposited onto mica in the presence of Ca^{2+} (500 μM). Under these conditions, the liposomes collapse and merge to form a single supported bilayer. When the liposomes were prepared from dioleoylphosphatidylcholine (DOPC) only, the resultant bilayer was smooth and featureless (Figure 2A). There were occasional gaps in the bilayer (e.g., dark area at the bottom right of Figure 2A), and a section through the bilayer revealed that the step in height down to the mica support was 5.8 nm (Figure 2B). The expected thickness of a lipid bilayer composed of DOPC is 3.5 nm (36). The additional thickness is likely due to the presence of a hydration layer between the bilayer and the mica; such a layer has been reported previously (37). Bilayers composed of DOPC and phosphatidylserine (PS) (3:1) were similarly featureless (Figure 2C) and now had a height step down to the mica support of 4.8 nm, likely indicating a closer interaction between the PS-containing bilayer and the mica (Figure 2D).

To study the interaction of C2AB with lipid bilayers, liposomes were preincubated with a low concentration of the protein (2.5 nM), and then supported bilayers were produced. Free C2AB was washed away before AFM imaging. When liposomes composed of DOPC were incubated with C2AB in the presence of Ca^{2+} (500 μM), the resulting bilayer was almost featureless (Figure 3A), which was seen with DOPC bilayers produced in the absence of protein (Figure 2A). Figure 3B shows an image of a bilayer composed of DOPC and PS (3:1) that had been preincubated with C2AB in the absence of Ca^{2+}. Again, few features were seen on the bilayer, as in the absence of protein (Figure 2C). In contrast, when the same experiment was repeated in the presence of Ca^{2+} (500 μM), the bilayer was now decorated with many raised features of various sizes (Figure 3C). Note also the presence of a large number of small particles attached to the uncoated areas of mica. These are presumably C2AB molecules primarily in dimeric form, as seen in Figure 1B. The lipid-bound particles are clearly larger than those attached to the mica and must therefore represent oligomers.

Figure 4 illustrates the interaction of C2AB, at a high concentration (1 μM), with bilayers containing DOPC and PS at two molar ratios (3:1 and 1:1). When the DOPC:PS ratio was 3:1, there was a heterogeneous array of particles attached to the bilayer (Figure 4A). A molecular volume distribution of the bound particles is shown in Figure 4B. The peak of the distribution was at a molecular volume of 588 nm^3. In a previous electron microscopic study of C2AB bound to lipid monolayers, structures were observed that appeared to be barrel-shaped heptamers of the C2AB molecule (32). Interestingly, the size of the molecular volume peak obtained in our study would be consistent with structures of this type (predicted size of a monomer = 80 nm^3; 7×80 $nm^3 = 560$ nm^3). However, our data indicate that the bound protein particles are rather variable in size. Figure 4A also shows the presence of very large structures (> 50 nm wide), which are likely to be liposomes bound to the bilayer but not fused (which were seen only rarely on protein-free bilayers). In an attempt to distinguish between these liposomes and bound C2AB particles, we routinely applied an arbitrary cutoff at 3000 nm^3 to all of our molecular volume analyses. When the DOPC:PS ratio was 1:1, the binding density of C2AB was increased (Figure 4C), and the peak particle size increased from 588 to 951 nm^3. These results emphasize the importance of PS in mediating the binding of C2AB to the lipid bilayer and are also consistent with a previous study indicating that C2 domain-containing proteins affect the distribution of PS within the plane of the bilayer, recruiting the lipid and binding to it in the form of protein

patches (38). This previous study would predict that the mean particle size should increase along with the proportion of PS in the bilayer, which is what we observed. Some of the larger structures associated with the bilayer appeared as large, flat sheets. At higher magnifications, these sheets appeared to consist of two-dimensional aggregates of globular particles (data not shown). Note that our observation of aggregation of C2AB contrasts with the results of a previous study (26), which found no evidence of aggregation of C2AB on liposomes, using an assay based on fluorescence resonance energy transfer. One possible explanation of this discrepancy is that C2AB interacts differently with planar bilayers (as in our experiments) and liposomes.

Closer inspection of images obtained in the presence of C2AB, PS, and Ca^{2+} revealed another feature that was absent when no C2AB binding occurred: the presence of many indentations in the surface of the supported bilayer (e.g., compare Figure 4A with Figure 2C). Further information about the origin of these indentations was obtained from repeated scanning of bilayers decorated with C2AB. Panels A and B of Figure 5 are images of the same area of a bilayer taken in successive scans, approximately 7 min apart. The protein binding pattern was very similar between the two scans. However, a small number of the particles were lost between scans (indicated by arrows). In many cases, when a protein dissociated it left behind an indentation in the bilayer. This effect is shown at a higher magnification in panels C and D of Figure 5. A section was taken through a bound particle and an indentation (Figure 5E); the height profile along this section is shown in Figure 5F. As one can see, this particular indentation is ~45 nm in diameter and ~1.4 nm deep; it also has a lip around its edge (visible in the vertical cross section). Section analysis of 60 such indentations (all of similar diameters) gave a mean depth (±SD) of 1.81 ± 0.67 nm. The geometry of the scanning tip (tip radius of <10 nm) is such that it ought to be able to access the bottom of an indentation with a diameter of ~40 nm, even if it is actually a hole all the way through the bilayer to the mica support (4.8 nm deep). The fact that the observed depth is only 1.81 nm, therefore, indicates that the indentation does not completely span the bilayer.

Our ability to identify indentations in the bilayer in the positions previously occupied by bound C2AB particles indicates that the mobility of the particles (and the indentations) in the plane of the bilayer is restricted. We have seen this restricted mobility previously when we imaged sphingomyelin/cholesterol-enriched domains in a DOPC bilayer (39). The shapes of the domains were largely preserved in successive scans but changed dramatically, even during the course of a single scan, in response to manipulation of the cholesterol content of the bilayer. Other workers have shown that influenza M2, a small tetrameric protein with a molecular mass of 50 kDa, diffuses freely within the plane of a supported lipid bilayer (40). The C2AB particles imaged here are larger and are therefore likely to move more slowly on the bilayer. In addition, the effect of Ca^{2+} on the PS-containing bilayer is likely to be significant. For instance, it has been shown by others that Ca^{2+} triggers a strong interaction between bilayer PS and the mica support (41) and can even cause the flipping of PS into the leaflet of the bilayer that is in contact with the mica (42). It is likely that these effects would considerably reduce the mobility of features in the bilayer, such as the indentations. We should emphasize that we cannot exclude the possibility that there is a population of monomeric C2AB that is moving so rapidly that it escapes detection by the scanning tip. We were interested in examining the stability of indentations in the bilayer, so we took successive scans of a suitable area. As shown in Figure 6, the same indentation was visible in successive scans taken 7 min apart (Figure 6A,B). However, the shape of the indentation and the vertical profile (Figure 6C,D) changed between scans. Note that the profile in Figure 6C shows that the indentation has a relatively flat bottom, ~3 nm deep, lending support to our assertion that the scanning tip is indeed able to access the indentation fully. Note also that proteins have disappeared from the bilayer between scans, but not all have left

indentations. Furthermore, the relative positions of the particles and holes have shifted a little between scans.

We next asked whether the individual C2 domains, C2A and C2B, were able to form aggregates on PS-containing bilayers and whether they too were able to induce the formation of indentations. As shown in panels A and B of Figure 7, C2A bound efficiently to bilayers in the presence of Ca^{2+} and formed both multimeric particles and large sheetlike structures with a typical thickness of 2 nm. In addition, many indentations were seen, often in close association with attached particles, which seemed to line the edge of the indentations. C2B also formed large aggregates on the surface of the bilayers (Figure 7C,D). These were often elongated structures rather than sheets. C2B, too, caused the formation of indentations. Depths of the indentations seen with the individual C2 domains were 2.33 ± 0.60 nm (SD; $n = 55$) for C2A and 2.14 ± 0.66 nm ($n = 61$) for C2B. Both of these values are significantly larger than the depth of the indentations seen with C2AB ($P < 0.001$ for C2A; $P < 0.01$ for C2B). How does the presence of bound C2AB lead to the formation of the indentations? One possibility is that C2AB could bind tightly to the bilayer, and the scanning tip could then exert sufficient lateral force to dislodge both the protein particle and some attached lipid. This process could leave behind an area where one leaflet of the bilayer had been removed. However, the generation of such areas of a relatively stable lipid monolayer is thermodynamically unlikely. Alternatively, the protein could locally disrupt the structure of the bilayer, to produce a patch that is thin and therefore detectable by the tip as a depression. Such a patch might be sufficiently stable to persist for some time after the protein itself has dissociated. There are at least two reasons for favoring the latter explanation. First, the scanning was carried out in tapping mode, which is specifically designed to exert minimal lateral force on the scanned objects. It is therefore unlikely that the tip is able to push the protein particles off the bilayer. Second, areas of the bilayer are seen in initial scans that have little bound protein but many indentations. An extreme example is shown in panels E and F of Figure 7. This structure was observed in the first scan of this area of bilayer and therefore could not have resulted from the removal of bound particles by the scanning tip. We suggest that the incubation of C2AB with the liposomes might have brought about the multiple indentation of the bilayer. When the free protein was subsequently washed away, the resulting bilayer might have had a relatively low level of protein binding but might contain many residual indentations.

Figure 8 shows the effect of two types of mutation on the interaction of C2AB with the supported lipid bilayer. Panels A and B of Figure 8 show the binding of C2AB harboring mutations in the Ca^{2+} binding regions of both C2A and C2B ($C2A_M$–$C2B_M$; see above). It is clear that the binding density was low, compared with that of wild-type C2AB (Figure 3C), and that the typical particle size was smaller. The frequency distribution of molecular volumes (Figure 8C) had two peaks, a sharp one at 120 nm^3 and a broader one at 240 nm^3, indicating the presence of mainly monomers and dimers. Note also that the bilayer was almost free of indentations. Panels D and E of Figure 8 show the binding of C2AB harboring a mutation in C2B in which two lysine residues (K326 and K327) in a normally positively charged region have been replaced with alanines [C2AB(KK); 11, 13, 22, 32]. As for the $C2A_M$–$C2B_M$ mutant, the binding density of C2AB(KK) was low, and the typical particle size was small; the peak of the frequency distribution shown in Figure 8F is 219 nm^3, consistent with a predominantly dimeric structure. Again, there are almost no indentations in the bilayer. The effect of mutations in the Ca^{2+} binding regions of the C2 domains on the interaction of C2AB with the supported lipid bilayer is unsurprising, since these regions are known to become embedded in the bilayer (9–11, 13, 18, 27–30), and the effects of these mutations on C2AB binding to liposomes are well-documented (e.g., ref 11). The effect of the KK mutation is more difficult to explain, especially as the polybasic region of C2B

where the two lysines reside is quite distant from the Ca^{2+}-binding loops and has been reported not to make intimate contact with the surface of the membrane (30).

To discover more about the role of the polybasic region in the binding of C2AB to lipids, we used a stopped-flow rapid mixing approach to compare the kinetics of lipid association and dissociation of C2AB(WT) and C2AB(KK). The assay uses fluorescence resonance energy transfer to monitor the interaction of naturally occurring tryptophan and tyrosine residues in C2AB with dansyl-PE in liposomes. The liposomes contained 5% dansyl-PE, 25% PS, and 70% DOPC, a composition similar to that of the supported lipid bilayers in most of the AFM imaging experiments. Note that in these kinetic experiments, synthetic PS was used instead of the brain-derived PS used in the AFM experiments. It has been shown previously that the behavior of C2AB with respect to bilayers containing these two types of PS is very similar (11). Panels A and B of Figure 9 show representative traces of the association kinetics of C2AB(WT) and C2AB-(KK), respectively, in the presence of Ca^{2+}. A plot of k_{obs} versus liposome concentration is shown in Figure 9C. This plot was used to determine k_{on}, k_{off}, and K_d, as described in Experimental Procedures (Figure 9D). Representative traces of the disassembly kinetics following removal of Ca^{2+} are shown in panels E and F of Figure 9. It was found that the assembly and disassembly kinetics of C2AB(WT) and C2AB(KK) were not significantly different ($P > 0.05$), in contrast to the large difference in their behavior in our AFM imaging experiments. Similar discrepancies have arisen previously in experiments designed to investigate the association of isolated C2B with PS-containing liposomes, and it has become clear that the reported behavior of C2B depends on the assay system used. For instance, it was found that C2B, immobilized as a GST fusion protein, binds radiolabeled liposomes only weakly in pull-down assays (5, 32), whereas C2B efficiently cosediments with liposomes (32). The effect of the KK mutation is also assay-dependent. For example, it had no effect on the interactions of C2B with PS-containing liposomes, as monitored using either fluorescence resonance energy transfer, a membrane penetration assay, or pull-down of radiolabeled liposomes, and yet it abolished the cosedimentation of C2B with liposomes (32). The same mutation also reduced the apparent Ca^{2+} affinity of C2AB for PS-containing liposomes, as measured in a cosedimentation assay (14), and compromised the ability of C2B to aggregate liposomes, leading to the proposal that the polybasic region might be involved in the anchoring of the synaptic vesicle membrane to the plasma membrane during exocytosis (26). To account for the discrepancies between the results produced using different assays, it has been suggested that cosedimentation of syt with liposomes requires an additional property (possibly the ability to aggregate) that depends on the polybasic region (32). In this context, it should be noted that, as in our experiments, the KK mutation abolished the oligomerization of C2AB on lipid monolayers, as visualized by electron microscopy (32). It should also be borne in mind that in the kinetic experiments, where the lipid:protein ratio is relatively high, most C2AB molecules will be bound to the membrane. Under these conditions, the small difference in the affinity of binding between C2AB(WT) and C2AB(KK) might not be detected. In contrast, in most of the AFM experiments, the lipid:protein ratio will be lower so that only a fraction of the C2AB molecules will be bound to the bilayer. Under these conditions, differences in behavior between C2AB(WT) and C2AB(KK) might be more obvious.

DISCUSSION

We have shown that syt associates with PS-containing lipid bilayers in the form of aggregates of varying stoichiometry. These aggregates are seen at both low (2.5 nM) and high (1 μM) concentrations of syt. Hence, aggregation appears to be independent of the extent of saturation of the bilayer by syt. In addition, the binding of syt to the bilayers caused the perturbation of the bilayer structure, producing relatively stable indentations. It has been shown previously, using changes in the emission characteristics of strategically

placed fluorescent probes, that both C2A and C2B are able to penetrate the bilayer in response to Ca^{2+} binding (9–11, 13, 18, 27). Specifically, loops 1 and 3 of both C2 domains dip into the bilayer in response to Ca^{2+} binding. Fluorescence quenching experiments revealed that the tip of C2A can penetrate to a depth of ~1.5 nm (9, 27), similar to the depth of the indentations seen with C2AB in our experiments. In addition, others have concluded, on the basis of studies using site-directed spin labeling of C2AB, that both C2 domains penetrate to a depth of ~1 nm (30).

Since it is known that perturbation of the bilayer structure can under some circumstances trigger the fusion of lipid bilayers (e.g., ref 43), the bilayer perturbation caused by C2AB might be significant with respect to the role of syt as a Ca^{2+} sensor for neurotransmitter release. It should be emphasized that there is a large difference between the conditions under which our experiments were conducted and those prevailing in vivo; for instance, in the nerve terminal, syt is anchored to the synaptic vesicle membrane through its transmembrane domain, rather than being free in solution, as in our studies. It is possible that during neurotransmitter release syt is targeted to the presynaptic plasma membrane through its interaction with the t-SNAREs and phosphatidylinositol 4,5-bisphosphate (13, 14, 22), and that in response to Ca^{2+} a cluster of syt molecules causes membrane destabilization at the site of vesicle docking, which then leads to membrane fusion.

Most other proteins studied by AFM in association with supported lipid bilayers by us (37, 44–46) and by others (e.g., refs 40 and 47) have not been reported to cause the indentations seen here with C2AB. Interestingly, however, the 50-kDa C-terminal region of the tetanus toxin heavy chain, which mediates the binding of the toxin to the ganglioside G_{T1b}, has recently been shown by AFM analysis to cause the formation of 40–80 nm diameter and 1.5 nm deep indentations in supported lipid bilayers (48). These indentations developed slowly (i.e., over ~12 h) and were very stable. Total internal reflection fluorescence microscopy conducted in parallel with the AFM analysis indicated that the toxin fragment was present within the indentations. The ganglioside binding region of this tetanus toxin fragment has a predominantly positively charged surface. Significantly, a number of previous studies have found that other polybasic molecules cause the production of indentations in lipid bilayers similar to those seen in our experiments. In some cases, for example with poly-L-lysine and poly(ethyleneimine), these features are actually transbilayer holes that have been shown to be associated with the permeabilization of the bilayers (49). In other cases, for example with diethylaminoethyldextran, the indentations are too shallow to completely penetrate the bilayer, as seen in our experiments (49). These polybasic molecules [e.g., poly-(amidoamine)] have also been found to line the edges of the indentations (50), as we have found, particularly with the isolated C2 domains. Furthermore, the binding of the polybasic antimicrobial peptide MSI-78 to dimyristoyl-*sn*-glycero-3-phosphocholine bilayers has been shown by AFM to cause thinning of the bilayer by just more than 1 nm (51). Of course, both C2 domains of syt have predominantly positively charged surfaces in their Ca^{2+}-bound states (4, 5). In addition, the C2B domain contains a prominent polybasic region (2, 3). Reduction of the positive charge on this region by the introduction of neutralizing mutations is known to interfere with syt's ability to support neurotransmitter release in vivo (14, 52, 53). In our experiments, these mutations significantly reduce both the level of association of C2AB with the supported lipid bilayers and the extent of generation of bilayer indentations. The importance of the positively charged surfaces of Ca^{2+}-liganded syt with respect to its ability to interact with bilayers and to function in vivo supports the suggestion that membrane perturbation by syt's C2 domains might be key to its physiological function.

REFERENCES

1. Katz, B. The release of neural transmitter substances. Springfield, IL: Thomas; 1969.

2. Chapman ER. Synaptotagmin: A Ca^{2+} sensor that triggers exocytosis? Nat. Rev. Mol. Cell Biol. 2002; 3:1–11.
3. Südhof TC. The synaptic vesicle cycle. Annu. Rev. Neurosci. 2004; 27:509–547. [PubMed: 15217342]
4. Ubach J, Zhang X, Shao X, Südhof TC, Rizo J. Ca^{2+} binding to synaptotagmin: How many Ca^{2+} ions bind to the tip of a C2 domain? EMBO J. 1998; 17:3921–3930. [PubMed: 9670009]
5. Fernandez I, Aracç D, Ubach J, Gerber SH, Shin O, Gao Y, Anderson RG, Südhof TC, Rizo J. Three-dimensional structure of the synaptotagmin 1 C2B-domain: Synaptotagmin 1 as a phospholipid binding machine. Neuron. 2001; 32:1057–1069. [PubMed: 11754837]
6. Brose N, Petrenko AG, Südhof TC, Jahn R. Synaptotagmin: A calcium sensor on the synaptic vesicle surface. Science. 1992; 256:1021–1025. [PubMed: 1589771]
7. Davletov BA, Südhof TC. A single C2 domain from synaptotagmin I is sufficient for high affinity Ca^{2+}/phospholipid binding. J. Biol. Chem. 1993; 268:26386–26390. [PubMed: 8253763]
8. Chapman ER, Jahn R. Calcium-dependent interaction of the cytoplasmic region of synaptotagmin with membranes. Autonomous function of a single C2-homologous domain. J. Biol. Chem. 1994; 269:5735–5741. [PubMed: 8119912]
9. Bai J, Earles CA, Lewis JL, Chapman ER. Membrane-embedded synaptotagmin penetrates *cis* or *trans* target membranes and clusters via a novel mechanism. J. Biol. Chem. 2000; 275:25427–25435. [PubMed: 10840045]
10. Bai J, Wang P, Chapman ER. C2A activates a cryptic Ca^{2+}-triggered membrane penetration activity within the C2B domain of synaptotagmin I. Proc. Natl. Acad. Sci. U.S.A. 2002; 99:1665–1670. [PubMed: 11805296]
11. Hui E, Bai J, Chapman ER. Ca^{2+}-triggered simultaneous membrane penetration of the tandem C2-domans of synaptotagmin I. Biophys. J. 2006; 91:1767–1777. [PubMed: 16782782]
12. Schiavo G, Gu Q-M, Prestwich GD, Söllner TH, Rothman JE. Calcium-dependent switching of the specificity of phosphoinositide binding to synaptotagmin. Proc. Natl. Acad. Sci. U.S.A. 1996; 93:13327–13332. [PubMed: 8917590]
13. Bai J, Tucker WC, Chapman ER. PIP_2 increases the speed of response of synaptotagmin and steers its membrane-penetration activity toward the plasma membrane. Nat. Struct. Mol. Biol. 2004; 11:36–44. [PubMed: 14718921]
14. Li L, Shin O-H, Rhee J-S, Aracç D, Rah J-C, Rizo J, Südhof TC, Rosenmund C. Phosphatidylinositol phosphates as co-activators of Ca^{2+} binding to C2 domains of synaptotagmin 1. J. Biol. Chem. 2006; 281:15845–15852. [PubMed: 16595652]
15. Li C, Ullrich B, Zhang JZ, Anderson RGW, Brose N, Südhof TC. Ca^{2+}-dependent and Ca^{2+}-independent activities of neural and nonneural synaptotagmins. Nature. 1995; 375:594–599. [PubMed: 7791877]
16. Chapman ER, Hanson PI, An S, Jahn R. Ca^{2+} regulates the interaction between synaptotagmin and syntaxin 1. J. Biol. Chem. 1995; 270:23667–23671. [PubMed: 7559535]
17. Schiavo G, Stenbeck G, Rothman JE, Söllner TH. Binding of the synaptic vesicle v-SNARE, synaptotagmin, to the plasma membrane t-SNARE, SNAP-25, can explain docked vesicles at neurotoxin-treated synapses. Proc. Natl. Acad. Sci. U.S.A. 1997; 94:997–1001. [PubMed: 9023371]
18. Davis AF, Bai J, Fasshauer D, Wolowick MJ, Lewis JL, Chapman ER. Kinetics of synaptotagmin responses to Ca^{2+} and assembly with the core SNARE complex onto membranes. Neuron. 1999; 24:363–376. [PubMed: 10571230]
19. Zhang X, Kim-Miller MJ, Fukuda M, Kowalchyk JA, Martin TFJ. Ca^{2+}-dependent synaptotagmin binding to SNAP-25 is essential for Ca^{2+}-triggered exocytosis. Neuron. 2002; 34:599–611. [PubMed: 12062043]
20. Tucker WC, Edwardson JM, Bai J, Kim H-J, Martin TFJ, Chapman ER. Identification of synaptotagmin effectors via acute inhibition of secretion from cracked PC12 cells. J. Cell Biol. 2003; 162:199–209. [PubMed: 12860971]
21. Tucker WC, Weber T, Chapman ER. Reconstitution of Ca^{2+}-regulated membrane fusion by synaptotagmin and SNAREs. Science. 2004; 304:435–438. [PubMed: 15044754]

22. Bai J, Wang C-T, Richards DA, Jackson MB, Chapman ER. Fusion pore dynamics are regulated by synaptotagmin•t-SNARE interactions. Neuron. 2004; 41:929–942. [PubMed: 15046725]
23. Bhalla A, Tucker WC, Chapman ER. Synaptotagmin isoforms couple distinct ranges of Ca^{2+}, Ba^{2+}, and Sr^{2+} concentration to SNARE-mediated membrane fusion. Mol. Biol. Cell. 2005; 16:4755–4764. [PubMed: 16093350]
24. Bhalla A, Chicka MC, Tucker WC, Chapman ER. Ca^{2+}-synaptotagmin directly regulates t-SNARE function during reconstituted membrane fusion. Nat. Struct. Mol. Biol. 2006; 13:323–330. [PubMed: 16565726]
25. Damer CK, Creutz CE. Synergistic membrane interactions of the two C2 domains of synaptotagmin. J. Biol. Chem. 1994; 269:31115–31123. [PubMed: 7983052]
26. Aracç D, Chen X, Khant HA, Ubach J, Ludtke SJ, Kikkawa M, Johnson AE, Chiu W, Südhof TC, Rizo J. Close membrane-membrane proximity induced by Ca^{2+}-dependent multivalent binding of synaptotagmin-1 to phospholipids. Nat. Struct. Mol. Biol. 2006; 13:209–217. [PubMed: 16491093]
27. Chapman ER, Davis AF. Direct interaction of a Ca^{2+}-binding loop of synaptotagmin with lipid bilayers. J. Biol. Chem. 1998; 273:13995–14001. [PubMed: 9593749]
28. Frazier AA, Roller CR, Havelka JJ, Hinderliter A, Cafiso DS. Membrane-bound orientation and position of the synaptotagmin I C2A domain by site-directed spin labeling. Biochemistry. 2003; 42:96–105. [PubMed: 12515543]
29. Rufener E, Frazier AA, Wieser CM, Hinderliter A, Cafiso DS. Membrane-bound orientation and position of the synaptotagmin I C2B domain determined by site-directed spin labeling. Biochemistry. 2005; 44:18–28. [PubMed: 15628842]
30. Herrick DZ, Sterbling S, Rasch KA, Hinderliter A, Cafiso DS. Position of synaptotagmin I at the membrane interface: Cooperative interactions of tandem C2 domains. Biochemistry. 2006; 45:9668–9674. [PubMed: 16893168]
31. Martens S, Kozlov MM, McMahon HT. How synaptotagmin promotes membrane fusion. Science. 2007; 316:1205–1208. [PubMed: 17478680]
32. Wu Y, He Y, Bai J, Ji S-R, Tucker WC, Chapman ER, Sui S-F. Visualization of synaptotagmin I oligomers assembled onto lipid monolayers. Proc. Natl. Acad. Sci. U.S.A. 2003; 100:2082–2087. [PubMed: 12578982]
33. Schneider SW, Lärmer J, Henderson RM, Oberleithner H. Molecular weights of individual proteins correlate with molecular volumes measured by atomic force microscopy. Pfluegers Arch. 1998; 435:362–367. [PubMed: 9426291]
34. Lu Y, Bazzi MD, Nelsestuen GL. Kinetics of annexin VI, calcium, and phospholipid association and dissociation. Biochemistry. 1995; 34:10777–10785. [PubMed: 7662658]
35. Fuson KL, Montes M, Robert JJ, Sutton RB. Structure of human synaptotagmin C2AB in the absence of Ca^{2+} reveals a novel domain association. Biochemistry. 2007; 46:13041–13048. [PubMed: 17956130]
36. Sprong H, van de Sluijs P, van Meer G. How proteins move lipids and lipids move proteins. Nat. Rev. Mol. Cell Biol. 2001; 2:504–513. [PubMed: 11433364]
37. Saslowsky DE, Lawrence J, Ren X, Brown DA, Henderson RM, Edwardson JM. Placental alkaline phosphatase is efficiently targeted to rafts in supported lipid bilayers. J. Biol. Chem. 2002; 277:26966–26970. [PubMed: 12011066]
38. Hinderliter A, Almeida PFF, Creutz CE, Biltonen RL. Domain formation in a fluid mixed lipid bilayer modulated through binding of the C2 protein motif. Biochemistry. 2001; 40:4181–4191. [PubMed: 11300799]
39. Lawrence JC, Saslowsky DE, Edwardson JM, Henderson RM. Real-time analysis of the effects of cholesterol on lipid raft behavior using atomic force microscopy. Biophys. J. 2003; 84:1827–1832. [PubMed: 12609884]
40. Hughes T, Strongin B, Gao FP, Vijayvergiya V, Busath DD, Davis RC. AFM visualization of mobile influenza A M2 molecules in planar bilayers. Biophys. J. 2004; 87:311–322. [PubMed: 15240466]

41. Richter RP, Brisson AR. Following the formation of supported lipid bilayers on mica: A study combining AFM, QCM-D, and ellipsometry. Biophys. J. 2005; 88:3422–3433. [PubMed: 15731391]
42. Richter RP, Maury N, Brisson AR. On the effect of the solid support on the interleaflet distribution of lipids in supported lipid bilayers. Langmuir. 2005; 21:299–304. [PubMed: 15620318]
43. Weinreb G, Lentz BR. Analysis of membrane fusion as a two-state sequential process: Evaluation of the stalk model. Biophys. J. 2007; 92:4012–4029. [PubMed: 17369418]
44. Geisse NA, Wäsle B, Saslowsky DE, Henderson RM, Edwardson JM. Syncollin homo-oligomers associate with lipid bilayers in the form of doughnut-shaped structures. J. Membr. Biol. 2002; 89:83–92. [PubMed: 12235484]
45. Saslowsky DE, Lawrence JC, Henderson RM, Edwardson JM. Syntaxin is efficiently excluded from rafts in supported lipid bilayers containing cholesterol. J. Membr. Biol. 2003; 194:153–164. [PubMed: 14502428]
46. Geisse NA, Cover TL, Henderson RM, Edwardson JM. Targeting of *Helicobacter pylori* vacuolating toxin to lipid raft membrane domains analysed by atomic force microscopy. Biochem. J. 2004; 381:911–917. [PubMed: 15128269]
47. Wagner ML, Tamm LK. Reconstituted syntaxin1A/SNAP25 interacts with negatively charged lipids as measured by lateral diffusion in planar supported bilayers. Biophys. J. 2001; 81:266–275. [PubMed: 11423412]
48. Slade AL, Shoeniger JS, Sasaki DY, Yip CM. In situ scanning probe microscopy studies of tetanus toxin-membrane interactions. Biophys. J. 2006; 91:4565–4574. [PubMed: 16997879]
49. Hong S, Leroueil PR, Janus EK, Peters JL, Kober M-M, Islam MT, Orr BG, Baker JR Jr, Banaszak Holl MM. Interaction of polycationic polymers with supported lipid bilayers and cells: Nanoscale hole formation and enhanced membrane permeability. Bioconjugate Chem. 2006; 17:728–734.
50. Mecke A, Majoros IJ, Patri AK, Baker JR Jr, Banaszak Holl MM, Orr BG. Lipid bilayer disruption by poly cationic polymers: The roles of size and chemical functional group. Langmuir. 2005; 21:10348–10354. [PubMed: 16262291]
51. Mecke A, Lee D-K, Ramamoorthy A, Orr BG, Banaszak Holl MM. Membrane thinning due to antimicrobial peptide binding: An atomic force microscopy study of MSI-78 in lipid bilayers. Biophys. J. 2005; 89:4043–4050. [PubMed: 16183881]
52. Mackler JM, Reist NE. Mutations in the second C2 domain of synaptotagmin disrupt synaptic transmission at *Drosophila* neuromuscular junctions. J. Comp. Neurol. 2001; 436:4–16. [PubMed: 11413542]
53. Loewen CA, Lee SM, Shin YK, Reist NE. C2B polylysine motif of synaptotagmin facilitates a Ca^{2+}-independent stage of synaptic vesicle priming in vivo. Mol. Biol. Cell. 2006; 17:5211–5226. [PubMed: 16987956]

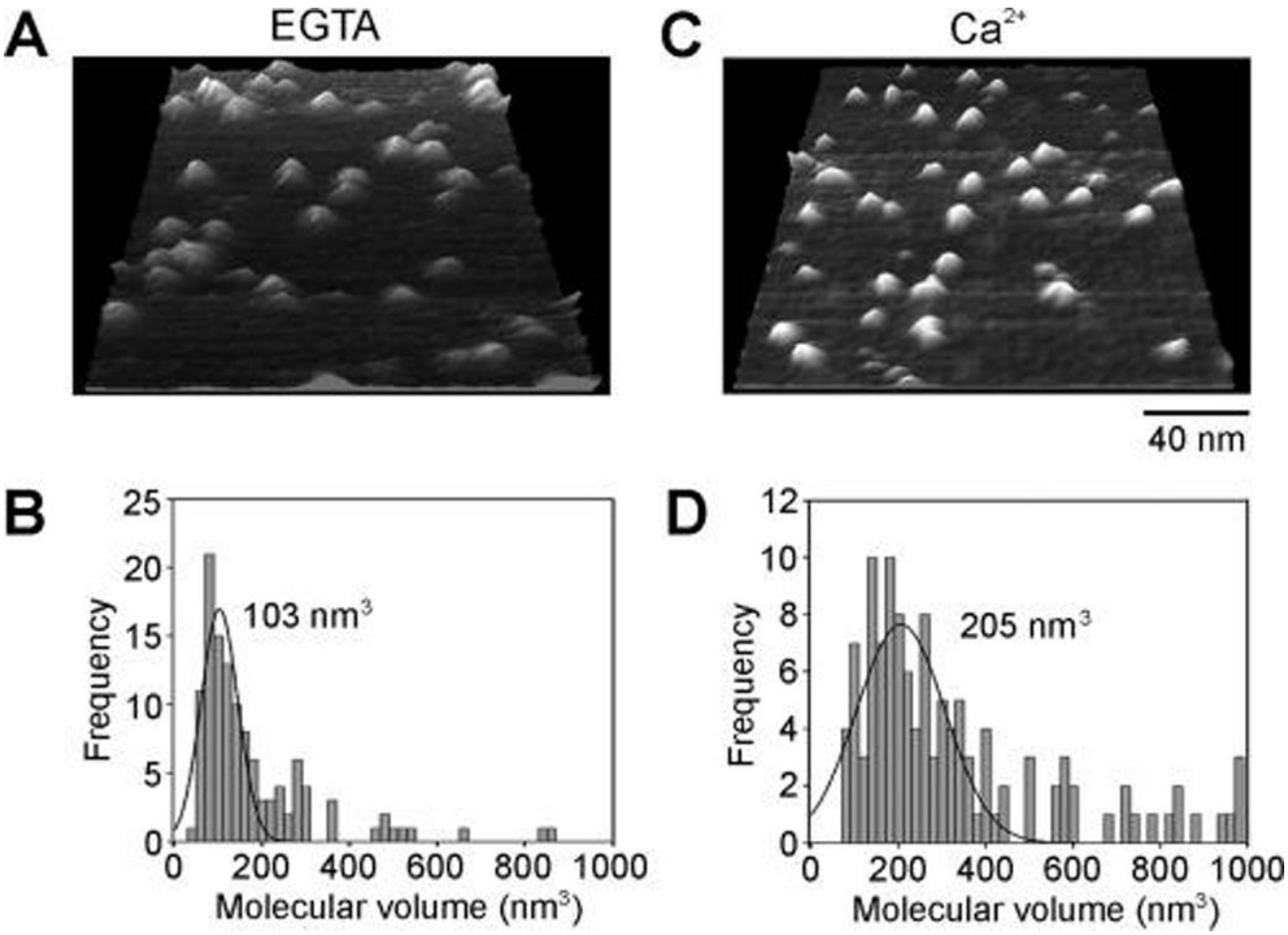

FIGURE 1.

Interaction of C2AB with mica. C2AB (2.5 nM) was incubated with mica in the presence of either EGTA (2 mM; A and B) or Ca^{2+} (500 μM; C and D) for 30 min. Free C2AB was then washed off, and the bound protein was imaged under fluid. Typical AFM images are shown in panels A and C. Molecular volumes of a number of particles were calculated from the particle dimensions, according to eq 1. Frequency distributions of the molecular volumes are shown in panels B and D. The peaks of the two distributions are indicated.

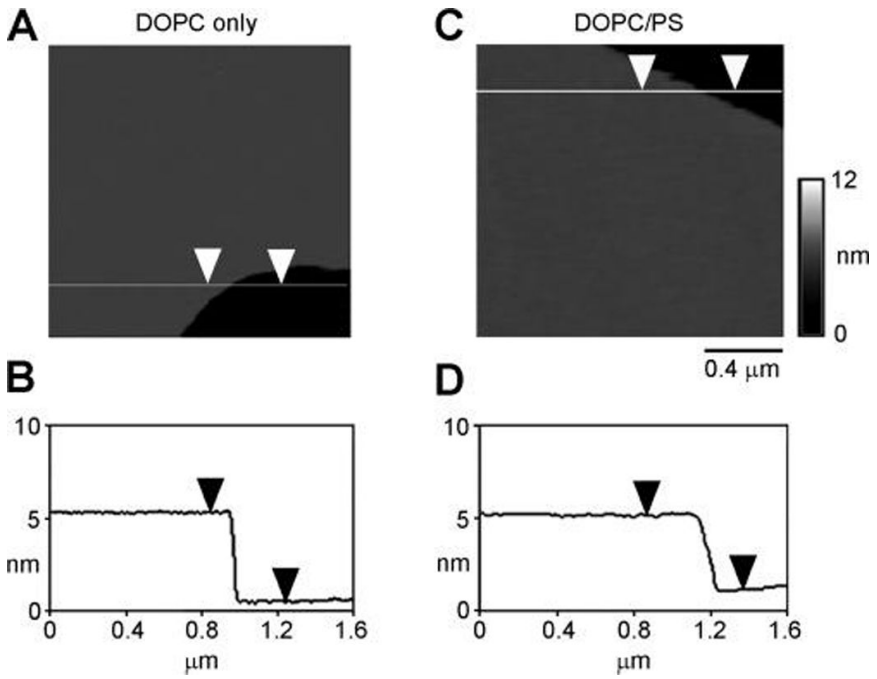

FIGURE 2.

Appearance of protein-free supported lipid bilayers. Liposomes composed of either DOPC only (A and B) or DOPC/PS (3:1; C and D) were deposited on mica in the presence of Ca^{2+} (500 μM), and the resulting supported lipid bilayers were imaged under fluid. Vertical cross sections (white lines) at the edge of the bilayers allow the heights of the bilayer to be determined: 5.8 nm in panel B and 4.8 nm in panel D. The shade-height scale refers to both panels A and C.

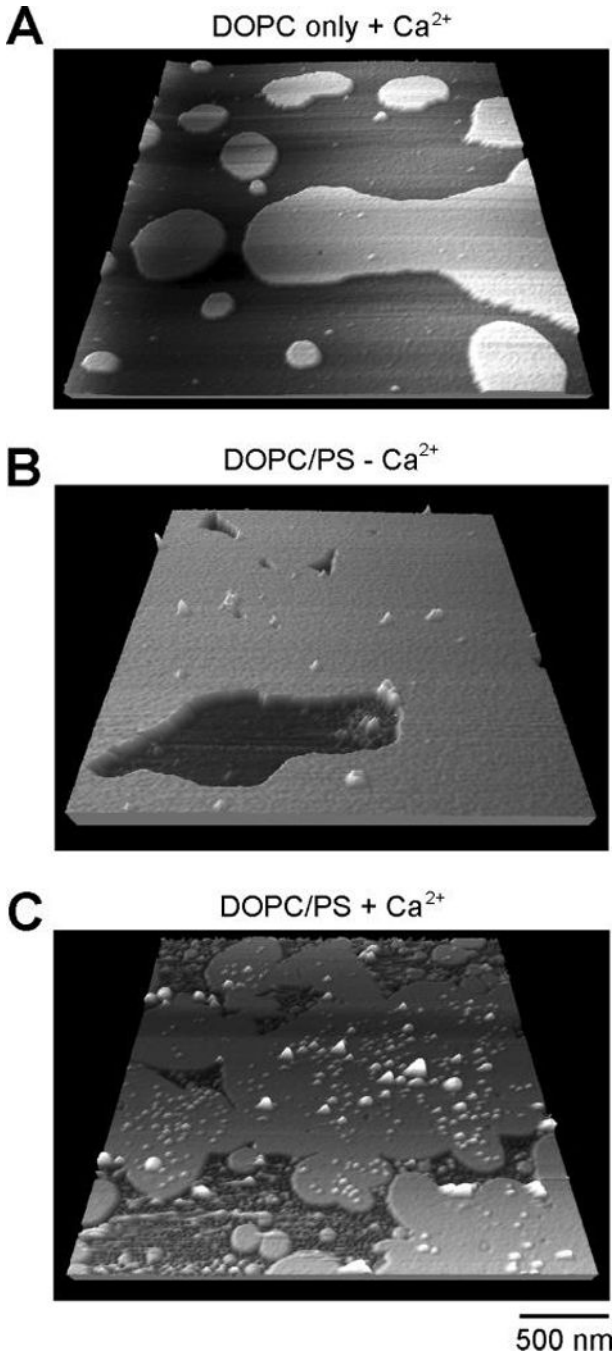

FIGURE 3.

Binding of C2AB to supported lipid bilayers requires both Ca^{2+} and PS. C2AB (2.5 nM) was incubated with DOPC-only liposomes in the presence of Ca^{2+} (500 μM; A), with DOPC/PS (3:1) liposomes in the presence of EGTA (2 mM; B), or with DOPC/PS liposomes in the presence of Ca^{2+} (C). The liposomes were deposited on mica to produce supported lipid bilayers, and the free C2AB was washed off. Bilayers were imaged under fluid. Typical images are shown. In contrast to panels A and B, many particles are bound to the bilayer in panel C. The largest particles (>50 nm wide) are likely to be unfused liposomes attached to the bilayer. Note that these, too, are largely absent in panels A and B.

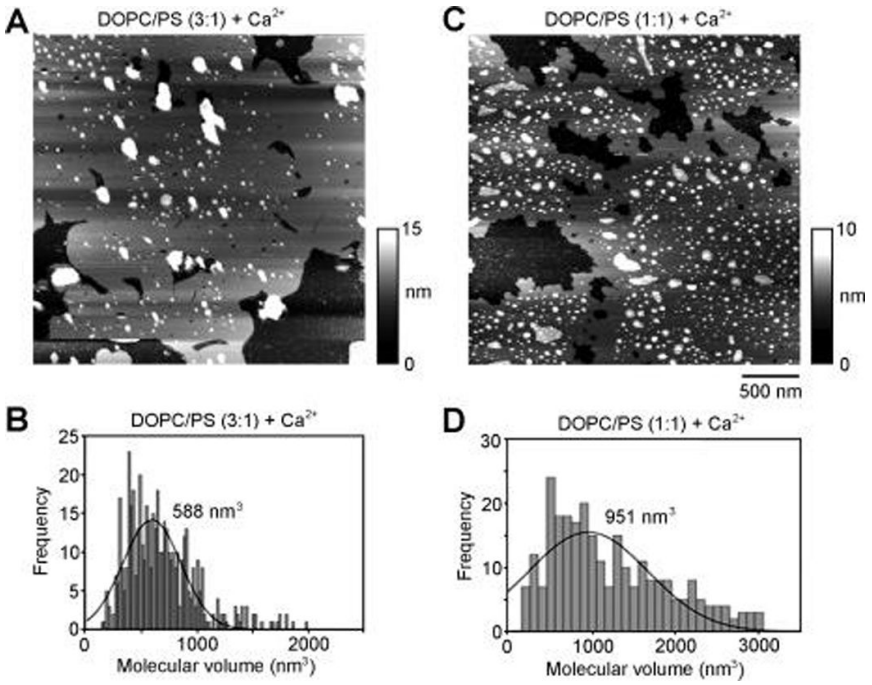

FIGURE 4.

PS content of the bilayer controls C2AB binding density and particle size. Supported lipid bilayers with bound C2AB (initial concentration of 1 μM) were produced from liposomes composed of DOPC and PS at ratios of 3:1 (A and B) and 1:1 (C and D). Typical images are shown in panels A and C. Note the presence of large sheetlike structures attached to the bilayer in panel C. (B and D) Frequency distributions of particle sizes. Peak molecular volumes are indicated.

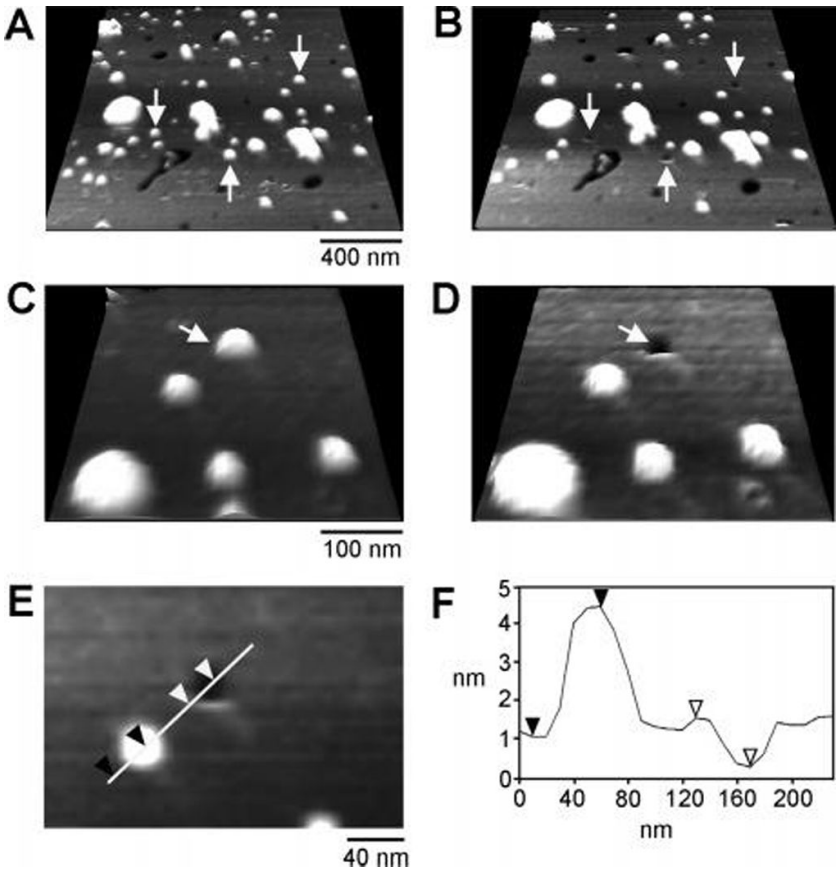

FIGURE 5.

Dissociating C2AB particles leave behind indentations in the bilayer. Supported lipid bilayers with bound C2AB (initial concentration of 1 μM) were produced from liposomes composed of DOPC and PS (3:1). (A and B) The same area of a bilayer was scanned twice, with a 7-min interval. The appearance of the bilayer in the two scans is very similar; however, several particles have dissociated from the bilayer, leaving behind indentations (arrows). (C and D) At a higher magnification, the result of the dissociation of one particle is shown (arrow). (E) A vertical cross section through a bound particle and an indentation was taken at the position of the white line. (F) The section indicates that the depth of the indentation is 1.4 nm.

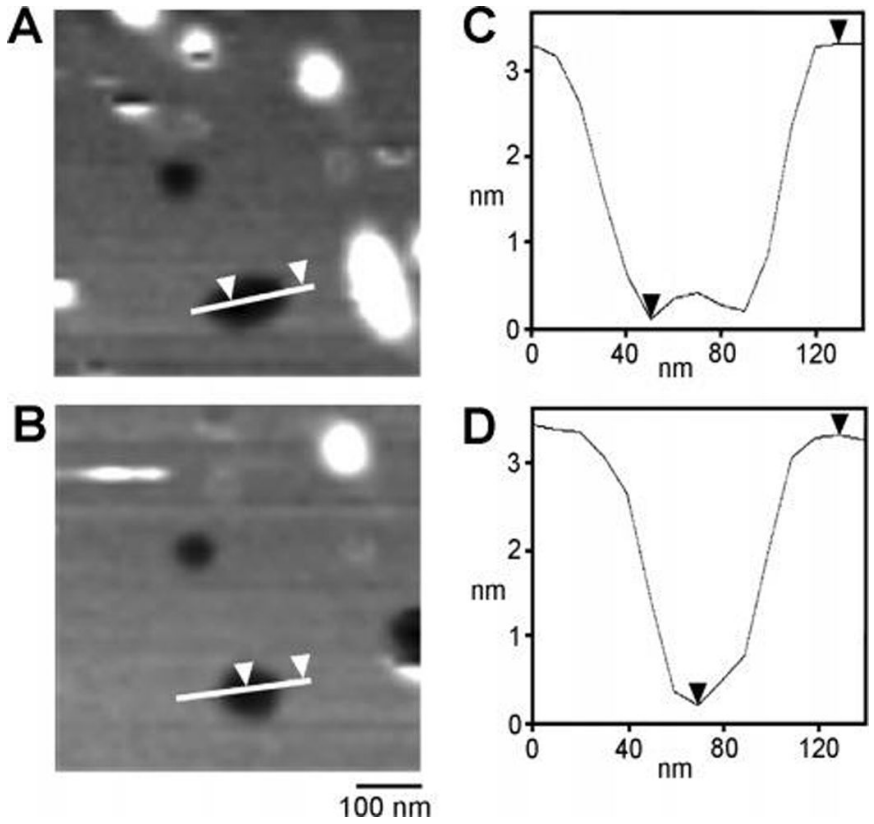

FIGURE 6.

Stability of the bilayer indentations. Supported lipid bilayers with bound C2AB (initial concentration of 1 μM) were produced from liposomes composed of DOPC and PS (3:1). A representative area of a bilayer was subjected to successive scans 7 min apart. (A and B) Several differences can be seen between the two images: the shape of the major indentation changes, some particles disappear from the bilayer, and the relative positions of the particles and holes shift slightly. (C and D) Vertical sections taken through the major indentation seen in the two successive scans. Note that the indentation initially has a rather flat bottom and that its profile changes between scans. The depth of the indentation is ~3 nm.

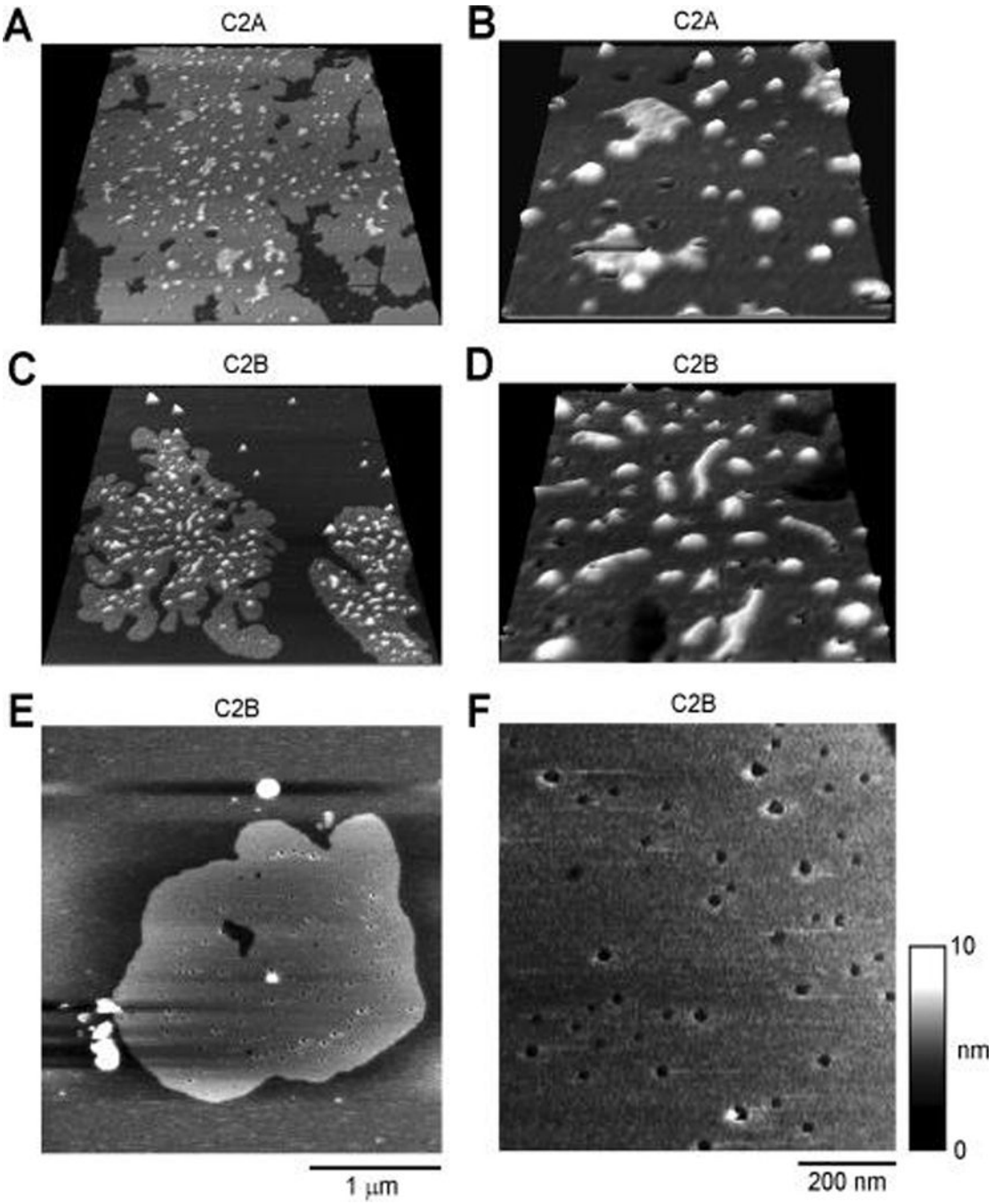

FIGURE 7.

Individual C2 domains cause bilayer indentations. Supported lipid bilayers with bound C2A (A and B) or C2B (C–F), at an initial concentration of 1 μM, were produced from liposomes composed of DOPC and PS (3:1). (A and B) Low- and high-magnification images of a bilayer showing bound C2A. Note the presence of both globular particles and flat sheetlike structures. Indentations in the bilayer are clearly visible, often in association with bound material. (C and D) Low- and high-magnification images of a bilayer showing bound C2B. Note the presence of both globular particles and wormlike structures. Again, indentations are often associated with bound material. (E and F) Low- and high-magnification images of an area of bilayer that had been exposed to C2B containing numerous indentations but no

bound particles. The scale bars refer to all images on either the left or the right. The shade-height scale refers to panels E and F.

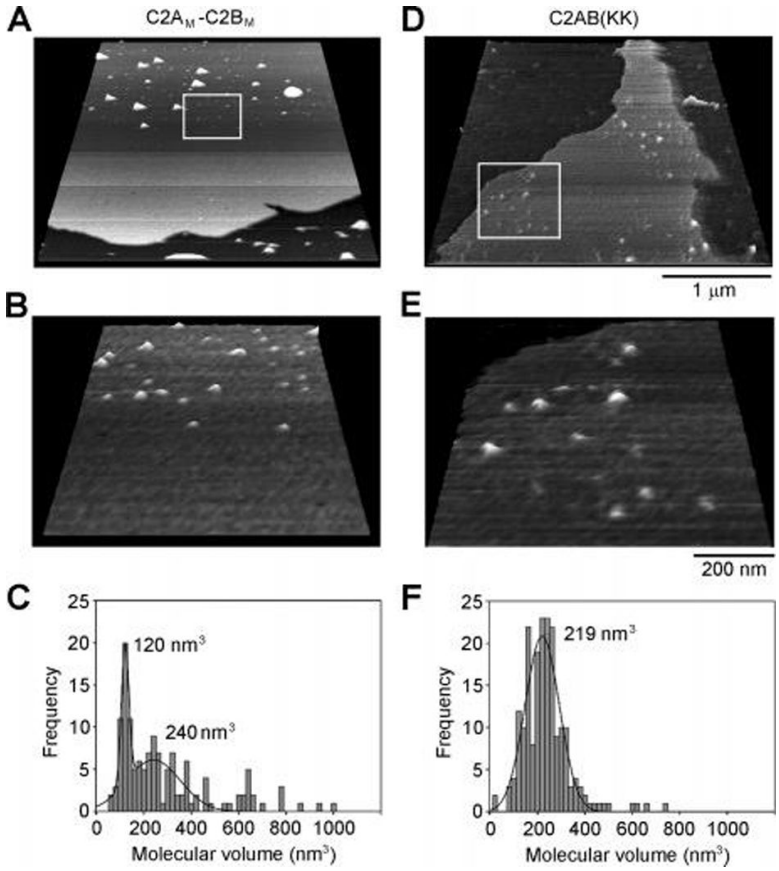

FIGURE 8.

Mutations in C2AB perturb its interaction with the bilayer. Supported lipid bilayers were produced from liposomes composed of DOPC and PS (3:1) that had been incubated with C2AB (initial concentration of 1 μM) bearing mutations in the Ca^{2+} binding regions of both C2A and C2B domains ($C2A_M$–$C2B_M$; A–C) or in the positively charged region of C2B [C2AB(KK); D–F]. (A and B) Images of an area of a bilayer showing a small number of bound $C2A_M$–$C2B_M$ particles. Panel B shows a high-magnification image of the boxed area in panel A. Note the almost complete absence of indentations. (C) Frequency distribution of the molecular volumes of the bound $C2A_M$–$C2B_M$ particles. The peaks of the distribution are indicated. (D and E) Images of an area of a bilayer showing a small number of bound C2AB(KK) particles. Panel E shows a high-magnification image of the boxed area in panel D. Again, note the almost complete absence of indentations. (F) Frequency distribution of the molecular volumes of the bound C2AB(KK) particles. The peak of the distribution is indicated.

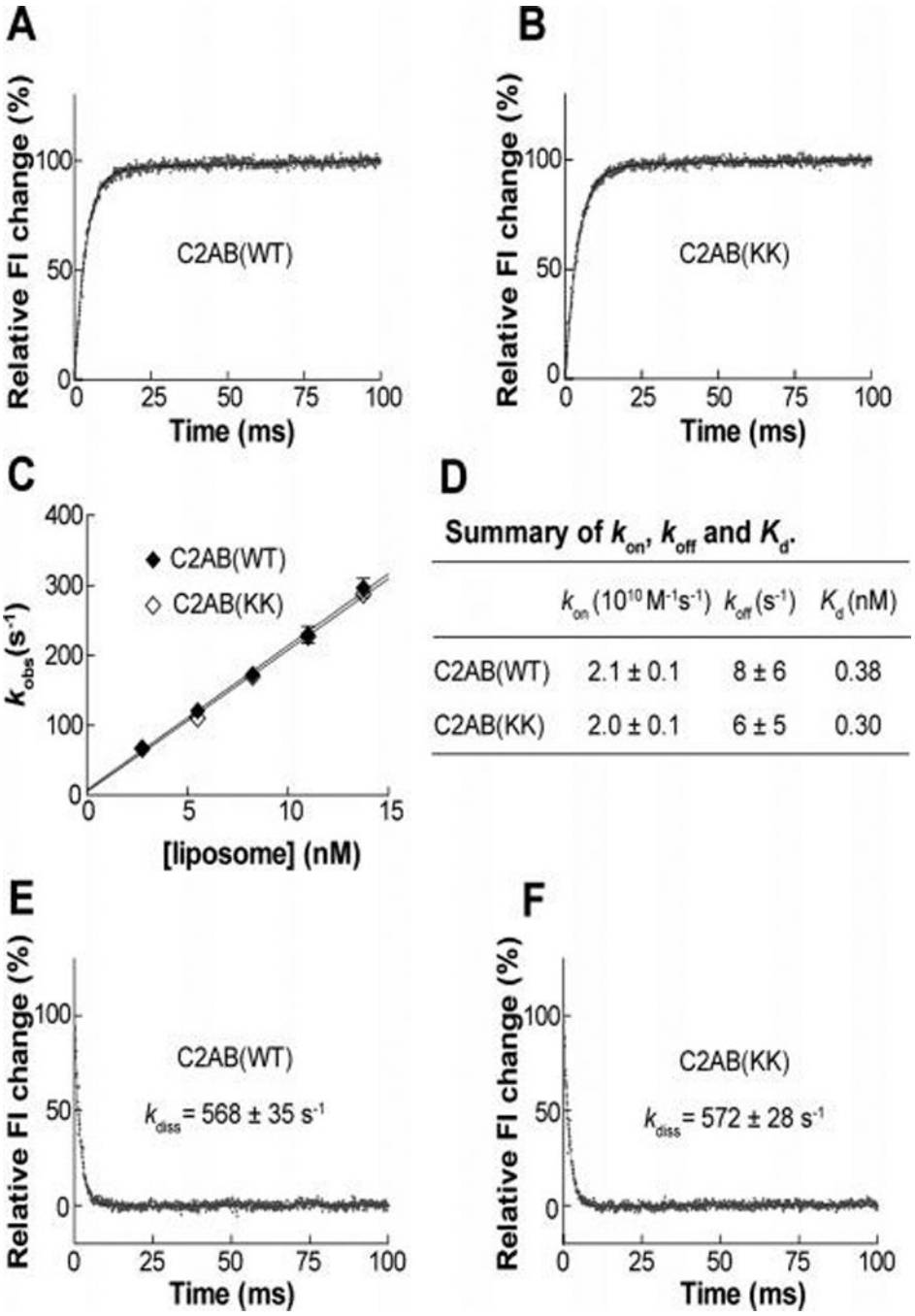

FIGURE 9.

Kinetic analysis of the interaction of C2AB with lipids. (A) Representative trace of the kinetics of Ca^{2+}-triggered C2AB-(WT)–liposome association (FI denotes fluorescence intensity). (B) Representative trace of the kinetics of Ca^{2+}-triggered C2AB(KK)–liposome association. (C) k_{obs} was determined by fitting the kinetic traces with a single-exponential function and was then plotted as a function of liposome concentration. The *y* intercept yields the off-rate constant (k_{off}), and the slope yields the on-rate constant (k_{on}) for the interaction of C2AB with PS-containing membranes in the presence of Ca^{2+}. Error bars represent SDs of three independent experiments. Values of k_{on} and k_{off} for C2AB(WT) and C2AB-(KK) are not significantly different ($P > 0.05$). (D) Summary of the values of k_{on}, k_{off}, and the

dissociation constant (K_d). (E) Representative trace of the disassembly kinetics of the C2AB(WT)–liposome complex. The rate constant for the fluorescence change, k_{diss}, was calculated by fitting the kinetic traces with a single-exponential function. (F) Representative trace of the disassembly kinetics of the C2AB(KK)–liposome complex. Values of k_{diss} for C2AB(WT) and C2AB(KK) are not significantly different.